ELSEVIER

Polymer 43 (2002) 3661–3674

polymer

www.elsevier.com/locate/polymer

# Toughening of isotactic polypropylene with $CaCO_3$ particles

Y.S. Thio[a], A.S. Argon[a], R.E. Cohen[a,*], M. Weinberg[b]

[a]*Massachusetts Institute of Technology, Cambridge, MA 02139, USA*
[b]*E.I. duPont de Nemours Co., Central Research and Development, Experimental Station, Wilmington, DE 19898, USA*

Received 20 November 2001; received in revised form 1 March 2002; accepted 4 March 2002

**Abstract**

The mechanisms of deformation and fracture of isotactic polypropylene filled with $CaCO_3$ particles were studied. Three types of particles with average diameters of 0.07, 0.7, and 3.5 μm were used at filler volume fraction from 0.05 to 0.30. The experiments included slow tensile tests, notched Izod impact tests with varying notch depths, and fracture resistance tests using double-cantilever-beam sample configurations. In slow tension, addition of fillers increased the modulus and decreased the yield stress independently of filler type. The strain at break increased with initial incorporation of fillers but decreased at higher loadings. The 0.7 μm diameter particles improved Izod impact energy up to four times that of the unfilled matrix. The other particles had either adverse or no effect on the impact toughness. The toughening mechanisms at work were plastic deformation of interparticle ligaments following particle–matrix debonding with additional contribution coming from crack deflection toughening. The failure of the 0.07 and 3.5 μm diameter particles to toughen the matrix was attributed to poor dispersion. © 2002 Published by Elsevier Science Ltd.

*Keywords*: Isotactic polypropylene; Calcium carbonate; Notched Izod impact toughening

## 1. Introduction

The challenge of improving the impact toughness of semicrystalline polymers continues to receive considerable interest. Among the polymers studied extensively is isotactic polypropylene (iPP) whose relatively ductile behavior at ambient condition readily degenerates at low temperatures and in the presence of notches. Among the different methods used to alleviate brittleness, the addition of rubber has been the most successful [1] although with the well-known shortcoming of decreased overall stiffness. Conversely, rigid fillers are commonly used to improve the modulus of the matrix usually with the penalty of decreased impact toughness. Of these mineral fillers, calcium carbonate ($CaCO_3$) is most commonly used mainly for its availability in readily usable form and low cost [2]. The trend seems to favor spherical sub-micron particles because of concerns over crack initiation by large irregularly shaped particles. The use of $CaCO_3$ to induce a modest toughening of iPP has been reported, although there is no general consensus on the mechanism of toughening [3–6].

Several frameworks and models have been proposed to explain the toughening effect on semicrystalline polymer. One such framework of particular interest to us is the concept of critical interparticle distance proposed by Wu [7], where a pronounced brittle-to-ductile transition is predicted to occur when the average distance between filler particles is lower than a critical value characteristic of individual polymers. An explanation for this phenomenon was offered by Muratoglu et al. [8] who showed in their work with Nylon-6 that toughening is produced by preferential orientation of crystal planes of the lowest shear resistance between filler particles. This phenomenon was shown to occur when the particles are sufficiently close together. The special crystallographic orientation in ligaments is expected to lower the local plastic resistance, leading to an increase in macroscopic ductility if the favorable behavior percolates throughout the material. Although the concept was originally proposed for rubber-toughened nylon matrix only, it was shown by Bartczak et al. to apply also to high density polyethylene filled with $CaCO_3$ particles [9–11]. The applicability to systems with other types of filler particles might be expected since the crystallite orientation phenomenon was demonstrated to occur both on rubber and calcite substrates. In addition to the critical interparticle distance, two other requirements were stated as important: (1) filler dispersion must be very regular to avoid creation of crack-initiating large agglomerates, 2) matrix–particle debonding must occur to allow unhindered plastic deformation around the particles.

These additional considerations were clarified in a recent

* Corresponding author. Tel.: +1-617-253-3777; fax: +1-617-253-9695.
*E-mail address:* recohen@mit.edu (R.E. Cohen).

0032-3861/02/$ - see front matter © 2002 Published by Elsevier Science Ltd.
PII: S0032-3861(02)00193-3

Table 1
Characteristics of calcium carbonate particles (properties were supplied by the manufacturer, Specialty Minerals Inc.)

| Code | Trade name | Density (g/cm$^3$) | Nominal mean diameter (μm) | Preparation | Surface area (m$^2$/g) | Calcium stearate added |
|---|---|---|---|---|---|---|
| CC0.07 | Ultrapflex | 2.7 | 0.07 | Precipitated | 19 | Unspecified |
| CC0.7 | Superpflex 200 | 2.7 | 0.7 | Precipitated | 7 | 2 wt% |
| CC3.5 | Hipflex 100 | 2.7 | 3.5 | Ground | 3 | 1 wt% |

study [12] using $CaCO_3$-filled Nylon-6. Despite the toughenability of Nylon-6 with rubber, $CaCO_3$ failed to increase the impact resistance appreciably. The failure was attributed to incomplete debonding in the early phases of impact response and to the presence of large agglomerates due to poor dispersion. One general principle hypothesized in that study is that toughenability of a semicrystalline polymer by rigid fillers depends also on the intrinsic plastic response of the matrix material at the temperature of interest. Polymers with high plastic resistance are expected to be less readily toughenable.

In view of these previous works, iPP becomes an interesting polymer for study. One reason is to determine if the different crystallography lends itself to the toughening mechanism outlined by Muratoglu et al. Another question is whether iPP, whose plastic resistance at room temperature lies between those of polyethylene and Nylon-6, can overcome the problems that prevent Nylon-6 from being toughened by rigid fillers. Thus, the purpose of this work is to investigate the mechanisms of deformation and fracture of $CaCO_3$-filled iPP. While the toughenability of iPP using rubber has been demonstrated [13], the question remains whether the underlying mechanisms are transferable to systems comprised of the same matrix filled with rigid fillers.

## 2. Experimental procedure

### 2.1. Sample preparation

iPP Accpro 9346 from BP Amoco Polymers, Inc. was used. The original pellets have a melt flow index of 12 g/10 min (2.16 kg at 190 °C) and a density of 0.91 g/cm$^3$. The filler particles were calcium carbonate ($CaCO_3$) obtained from Specialty Minerals Inc. Their properties are listed in Table 1. All of the particles were coated with calcium stearate by the manufacturer; the amount of coating is listed in Table 1.

The polymer pellets and the $CaCO_3$ particles were fed into a twin-screw extruder using dual K-tron weight loss feeders at approximately 25 lbs/h. The extruder was a 30-mm Werner and Pfleider twin-screw extruder operated at a temperature of 225 °C and screw rotation rate of 200 rpm. The resulting pellets were injection molded in a 6 oz, 150-Ton Van Dorn injection molding machine. A general purpose screw was used in the barrel, which is kept at 225 °C. The molds were heated to 40 °C. Three types of specimens were made: dog-bone tensile bars with gauge length of 50 mm, width of 12.7 mm, and thickness of 3.2 mm (ASTM D638 Type I); flexural test bars with dimensions of 127 mm × 12.7 mm × 3.2 mm; and plaques with dimensions of 125 mm × 75 mm × 6.4 mm. The flexural bars and plaques were machined to make test specimens as described later.

### 2.2. Mechanical property measurements

The dog-bone tensile bars were conditioned at 100 °C in vacuum for 12 h prior to testing. The tests were done at room temperature using an Instron 4201 tensile test machine. The cross-head speed was 5 mm/min which corresponds to an initial strain rate of $1.67 \times 10^{-3}$ s$^{-1}$. Displacement was measured from cross-head position. For each specimen, three runs were performed.

The flexural bars were cut into two equal pieces. Of each pair, the portion closer to the injection molding die was made into an Izod impact specimen according to ASTM D256. Each impact specimen had dimensions of 63.5 mm × 12.7 mm × 3.2 mm and was notched using a TMI cutter to produce notches with radius of 0.254 mm and depth of 2.54 mm. Three other sets of samples were made with the same geometry but with different notch depths. Three non-standard notch depths were used: 1.91, 1.27, and 0.635 mm. The Izod impact test was run using a Tinius Olsen 892 impact test machine with pendulum speed at impact of 3.46 m/s. The entire set of samples mentioned earlier was tested at room temperature. In addition, some standard-notched samples of the CC0.7-filled blends were tested at elevated temperatures, 50 and 80 °C, respectively. For the ASTM standard tests four runs were performed for each blend, while three specimens were tested for the other notch depths.

Tests using special double-cantilever-beam specimens were performed to determine the *J*-integral toughness for each blend. The specimens were machined out of the 6.4 mm thick plaques. The sample geometry is shown in Fig. 1. On each side of the sample, a groove (0.5 mm deep 90° V-notch) was machined to constrain the crack growth along the median plane of the sample. The initial crack was further sharpened by a small cut using a razor blade. The tests were carried out using an Instron 4201 machine at a cross-head speed of 50 mm/min. Load-opening displacement data were collected from three runs for each specimen.

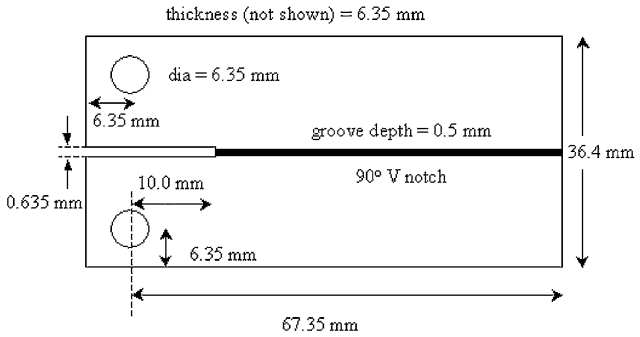


Fig. 1. Geometry of double-cantilever beam specimen for *J*-integral measurement.

### 2.3. Scanning electron microscopy

Specimens were examined using a Philips XL30 FEG scanning electron microscope (SEM), operated in a high vacuum mode ($\sim 10^{-8}$ bar). The accelerating voltage ranged from 3 to 10 kV. All SEM specimens were given a coating of gold/palladium of approximately 5 nm thickness to avoid charging and thereby improving image quality.

Undeformed molded specimens were examined by cryo-fracturing to obtain a survey of filler dispersion. For this purpose, the samples were given a sharp notch, immersed in liquid nitrogen for 10 min, and immediately cleaved by tapping a sharp blade placed at the notch. For samples where large agglomerates were found, micrographs at lower magnifications were taken to characterize the agglomerate size distribution. Subsequently, several micrographs at higher magnifications were obtained from the regions between agglomerates to obtain the individual particle size distribution. For each sample, the number of particles relative to that of clusters was calculated using the measured cluster-free area relative to the area of particle sampling, with the assumption that the size distribution of particles measured in those several regions is representative.

The SEM was also used to study the morphology of fracture surfaces of the Izod and tensile specimens. Additionally, deformed tensile specimens were cryo-fractured axially to reveal the morphology along the tensile direction.

## 3. Results

### 3.1. Dispersion of fillers in the iPP matrix

Molded specimens were cross-sectioned and examined under the SEM. The two precipitated particles (CC0.07 and CC0.7) were roughly spherical, while the ground particles (CC3.5) possessed irregular shapes with sharper edges. The size distribution of the ground particles was quite broad while, as can be expected from the production method, that of the precipitated particles was narrower. Particle and agglomerate size statistics are given in Table 2 for the lowest and highest loading of each particle type. The histograms are shown in Fig. 2.

The spatial dispersion was relatively good for the two larger fillers at filler volume fraction below 20%, above which many agglomerates were observed. The particles tend to agglomerate in large numbers, as few aggregates were found in the range 10–100 times the nominal average particle diameter. All the histograms show a bimodal distribution of size, except for the well-dispersed CC3.5 particles at low volume fraction. A large number of agglomerates were observed in the blends with CC0.07 particles, even at low volume fractions. The average agglomerate size also increased with increasing volume fraction, as shown in Table 2, suggesting further agglomeration during processing with the matrix.

### 3.2. Properties in slow tensile testing

The engineering stress–strain curves obtained from tension tests are presented in Fig. 3. Table 3 gives a summary of the properties of the blends. Predictably, the Young's moduli increased with increasing filler volume fraction. The increase was similar for similar volume fraction of particles independent of the choice of $CaCO_3$ fillers. For all three fillers, the yield stress (here taken as the peak stress) decreased with increasing particle volume fraction, indicating that the particles debonded prior to or at the start of plastic deformation. The evolution of the debonding process, starting from the 'shoulder' region and propagating to the 'necked' region, can be seen in the SEM micrographs of the tensile samples sectioned along stretching direction.

Table 2
Statistics of agglomerate and particle size based on SEM micrographs

| Particle | Particle vol% | Mean particle diameter[a] (μm) | Mean agglomerate diameter[b] (μm) | Agglomerate area% |
|---|---|---|---|---|
| CC0.07 | 5 | 0.16 | 47 | 6.3 |
| CC0.07 | 30 | 0.22 | 56 | 42.7 |
| CC0.7 | 10 | 0.37 | 28 | 3.5 |
| CC0.7 | 30 | 0.56 | 39 | 8.4 |
| CC3.5 | 5 | 2.88 | 12 | 0.1 |
| CC3.5 | 30 | 4.09 | 63 | 9.8 |

[a] Effective diameter of a circle of the same area taken up by a particle as observed on SEM.
[b] Only agglomerates/particles larger than 10 μm are included in this calculation.

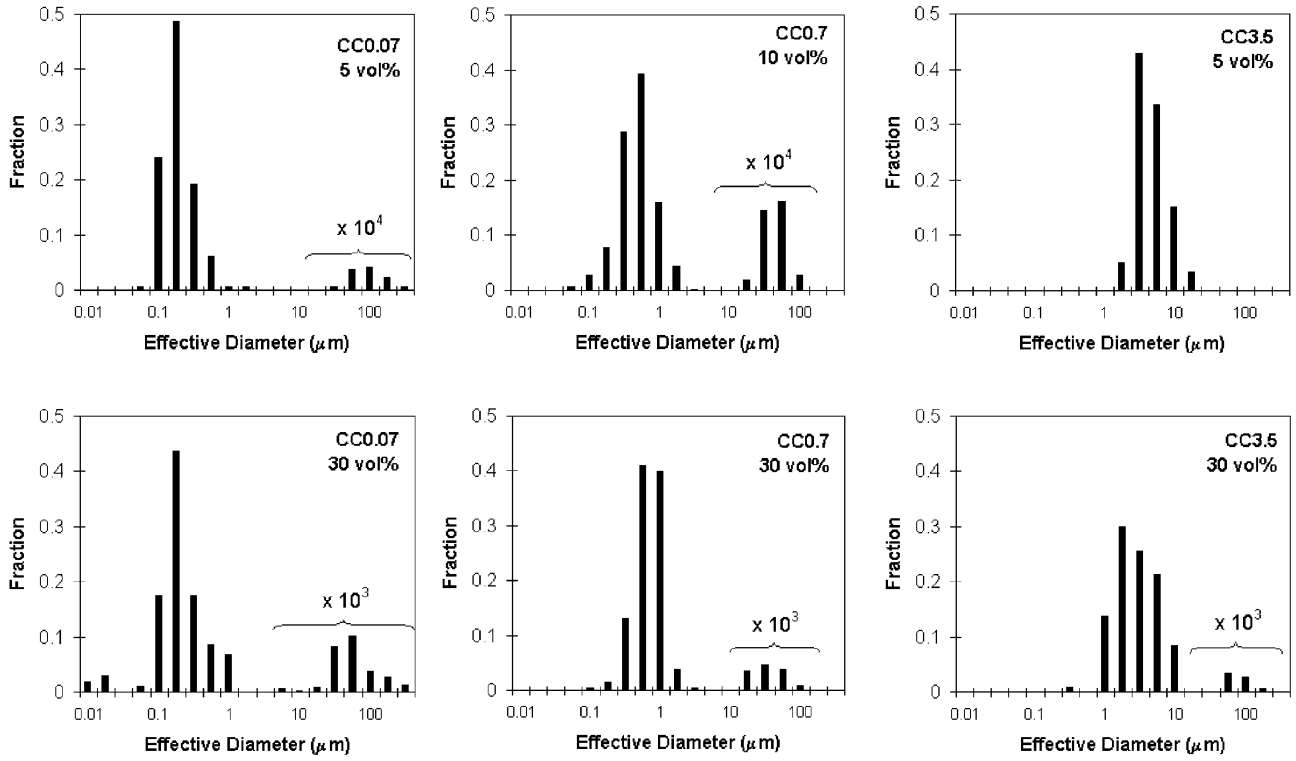


Fig. 2. Histograms of size distribution of the three different types of particles within the composites. The fraction of agglomerates are amplified for clarity by the factor given in each chart.

Fig. 4 is an example, representative of all the blends that showed necking, where the blend shown is iPP with 23.3 vol% CC0.7.

Several compounds demonstrated significantly higher strains-at-break than the unfilled iPP. Some of these stretched even to the limit of the testing machine, whereupon the test was discontinued. Smaller filler particles and higher volume fractions induced early fractures. In many cases during the test, whitened bands perpendicular to the tensile direction were observed at various locations on the samples. In compounds containing high filler concentrations, the whitened bands intensified and fracture occurred across one of them. In other cases, the bands coalesced and formed a larger band where a neck initiated. Closer examination of the whitened bands (Fig. 5) revealed that they indeed formed in regions with a large population of agglomerates.

The large particle agglomerates acted as sites for fracture

Table 3
Tensile properties of iPP/CC blends at room temperature and cross-head speed of 5 mm/min

| Mixture | Filler volume fraction | Young's modulus (MPa) | Peak stress (MPa) | Strain at break[a] (%) |
|---|---|---|---|---|
| iPP unfilled | 0 | 1437 | 33.1 | 121.4 |
| iPP/CC0.07 | 5 | 1691 | 27.2 | – |
| | 10 | 1871 | 25.1 | 87.4 |
| | 20 | 1973 | 21.5 | 13.7 |
| | 30 | 2697 | 19.2 | 5.9 |
| iPP/CC0.7 | 10 | 1682 | 27.4 | – |
| | 16.7 | 1785 | 25.9 | 494.7 |
| | 23.3 | 2440 | 22.9 | 230 |
| | 30 | 2867 | 20.5 | 13.4 |
| iPP/CC3.5 | 5 | 1629 | 27.1 | – |
| | 10 | 2050 | 25.5 | – |
| | 20 | 2294 | 21.6 | – |
| | 30 | 3057 | 17.3 | 147.8 |

[a] Unspecified strain at break indicates that the sample stretched up to the cross-head displacement limit of the Instron machine. In these cases, the tests were stopped prior to specimen fracture.

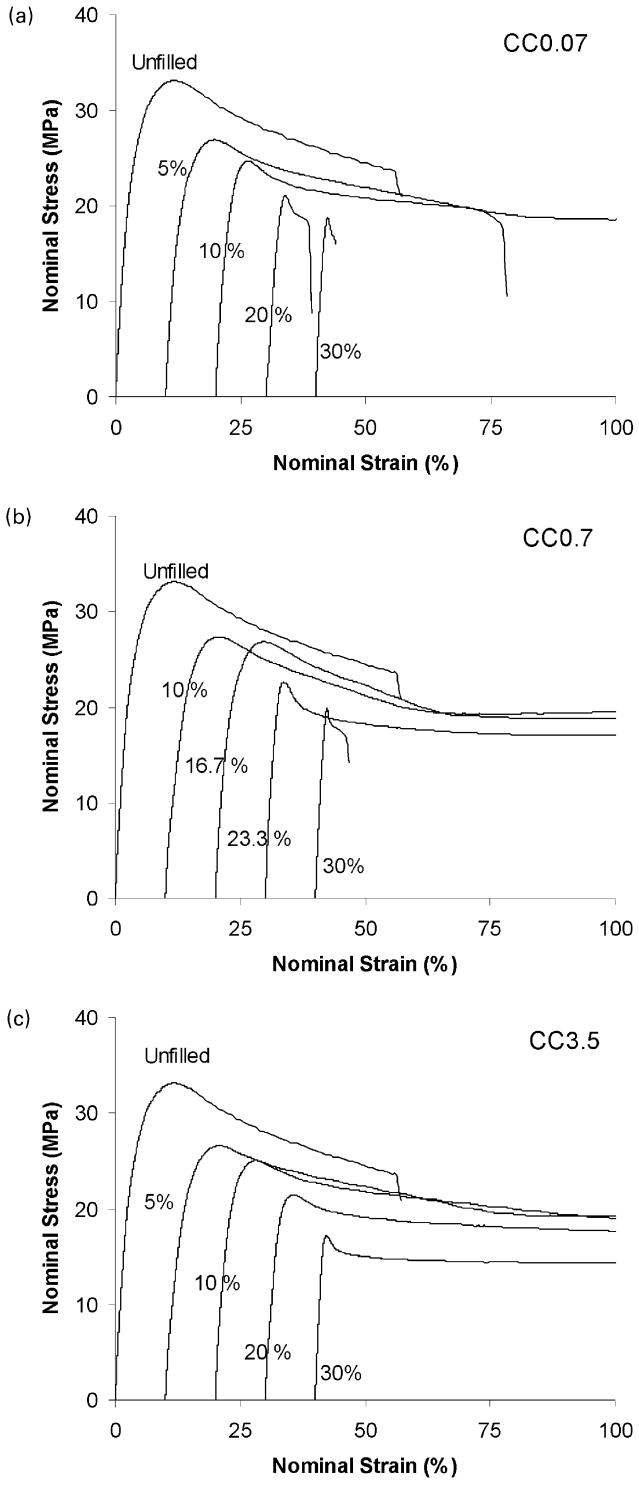


Fig. 3. Stress–strain curve of iPP blends with CC0.07, CC0.7, and CC3.5. Curves were shifted along the strain axis (increments of 10%) for clarity.

initiation. Whether or not the sample could survive such concentrated local deformation depends on the size, number, and internal constitution of these agglomerates. As mentioned earlier, clustering occurred more frequently with smaller particles and higher volume fraction. Fig. 6(a) shows a micrograph of the fracture surface of a tensile

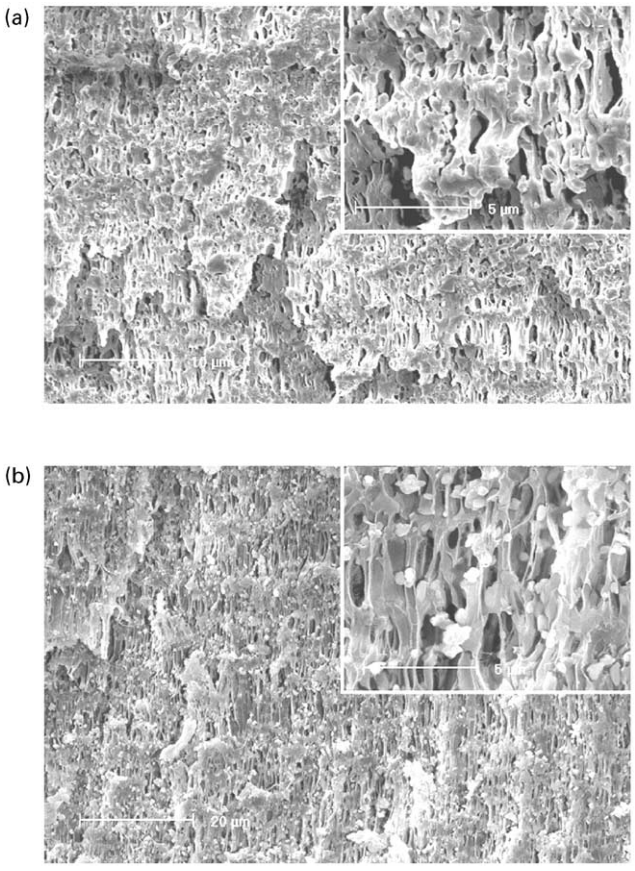


Fig. 4. SEM fractographs of iPP + 23.3 vol% CC0.7 tensile sample sectioned along the direction of deformation, showing evolution of debonding and plastic deformation around particles: (a) is taken from a region still undergoing deformation (shoulder) while (b) is from the fully deformed (neck) region. The inset micrographs give features at a larger magnification.

sample (iPP with 30% CC0.7) where brittle fracture originated from a large agglomerate following some ductile crack growth in the region surrounding the agglomerate. On the other hand, some samples were able to avoid catastrophic failure despite the presence of these agglomerates. Fig. 6(b) shows a view of an axial section along the tensile direction of another tensile sample (iPP with 23% CC0.7) where a large agglomerate, apparently still of sub-critical size, had not induced fracture. Rather, it acted as a single composite particle, debonded from the matrix, and did not inhibit extensive stretching of the matrix. Shown in Fig. 6(c) is another region from the same sample where an agglomerate did not debond but instead fractured into several parts that clung tightly to the matrix. The same phenomena were observed in the blends with CC0.07 particles.

### *3.3. J-integral work of fracture from double-cantilever-beam experiment*

A more quantitative method to characterize the crack growth resistance is to determine the *J*-integral toughness (*J*, given in units of energy per cracked area) from

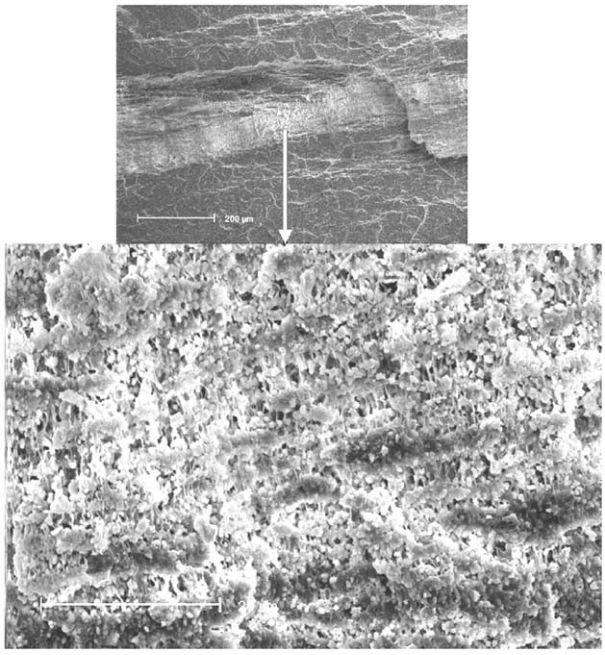

Fig. 5. SEM fractographs of whitened bands appearing in a tensile sample of iPP + 20 vol% CC0.07. The micrograph at higher magnification shows that deformation is concentrated in regions with high local filler content.

double-cantilever-beam experiments. The relevant equations characterizing $J$ are [14]

$$J = \alpha\varepsilon_0 Y_0(1-\phi)ch_1(a/b,n)(P/P_0)^{n+1} \quad (1)$$

$$P_0 = 1.072(\sqrt{1+a/c} - a/c)cY_0(1-\phi) \quad (2)$$

where $\alpha$, $\varepsilon_0$, $Y_0$, and $n$ are material constants with $\varepsilon_0$ being the yield strain; $Y_0$, yield stress; $n$, strain hardening exponent; $\phi$ is the filler concentration; $a$ is the effective crack length (as shown in Fig. 1), $b$ is the width of specimen, $c = b - a$; $h_1$ is a tabulated function of $n$ and $a/b$, obtained from numerical solutions of the crack tip field [14]; $P$ is the measured peak load per unit thickness, $t_s$, and $P_0$ are the plane-stress limit load.

The material constants were derived from fitting uniaxial compression data to the power-law strain-hardening expression, as detailed in Appendix A. The following values were obtained: $\alpha\varepsilon_0 = 0.0105$, $Y_0 = 16.0$ MPa, and $n = 2.16$. For the geometry-specific constants, the following values were used: $a = 10$ mm, $b = 67.4$ mm, $t_s = 5.35$ mm (taking into account the side grooves). Interpolation of tabulated values of $h_1$ [14] using the given $a$, $b$, and $n$ resulted in $h_1 = 1.83$.

The $J$-integral work of fracture was calculated for a given $\phi$ using the measured peak load. All the specimens show initially stable crack growth up to a certain peak load indicative of a relatively tough behavior. In several cases, especially in samples with low volume fraction of filler, the cracks became unstable. In these cases, the crack bifurcated before it reached the end of the specimen. The fact that the crack split in two opposing directions instead of veering to only one side is a strong indication of attainment of high crack velocity, which is characteristic of brittle response often due to a high level of triaxial tensile stress. The increased triaxiality resulted from crack blunting, which varied depending on the modulus and yield stress of each specimen. Even in these cases, however, the cracks had blunted and a peak load had been reached before brittle propagation was triggered, justifying the use of maximum load in the calculation of $J$. The results are given in Fig. 7.

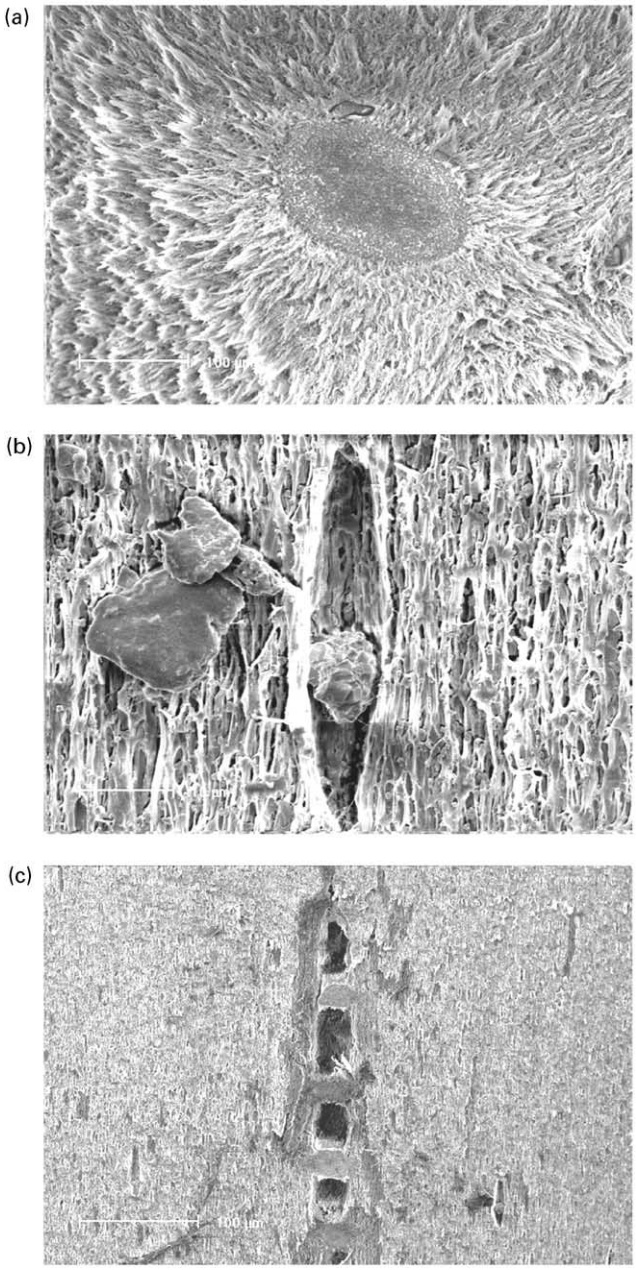


Fig. 6. SEM fractographs of tensile samples of iPP + CC0.7. (a) Fracture surface of a sample with 30 vol% filler showing a large agglomerate as the origin of fracture. (b) and (c) are axial sections along the direction of deformation from a sample with 23.3 vol% filler. (b) shows an agglomerate which behaves as a single particle, while (c) shows another possibility in which an agglomerate has fractured internally.

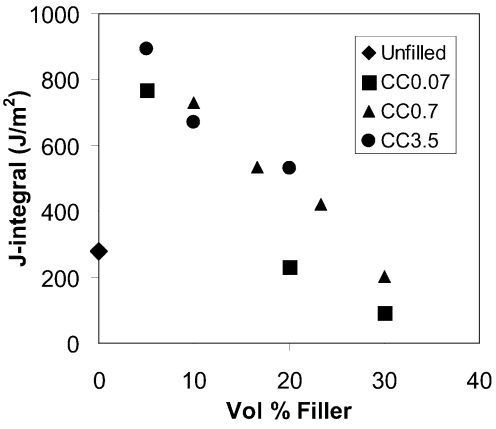


Fig. 7. *J*-integral value of the blends plotted against volume fraction of filler.

Independent of filler type, *J* at first increased with addition of $CaCO_3$ substantially above the unmodified iPP behavior. However, *J* decreased monotonically as filler concentration is increased further. The behavior parallels the slow tensile test results where the tensile toughness—the area under the stress–strain curve—first increased with initial addition of filler particles but then decreased with subsequent addition of filler.

### 3.4. Izod impact response

The impact energy values from standard Izod impact tests at room temperature are shown in Fig. 8. The blends with CC0.07 and CC3.5 showed impact energies close to the value for unfilled iPP. On the other hand, CC0.7 increased the impact energy considerably. Macroscopically, all the blends showed signs of brittle fracture behavior, where the

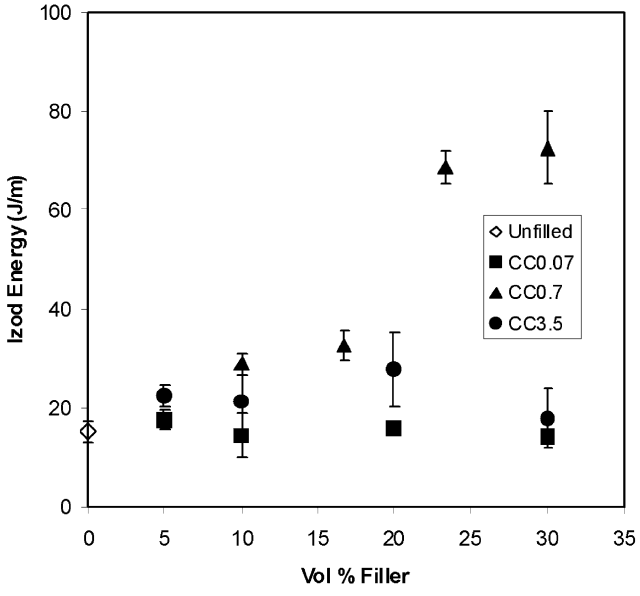


Fig. 8. Standard notched Izod impact energies of the blends at room temperature plotted against volume fraction of filler.

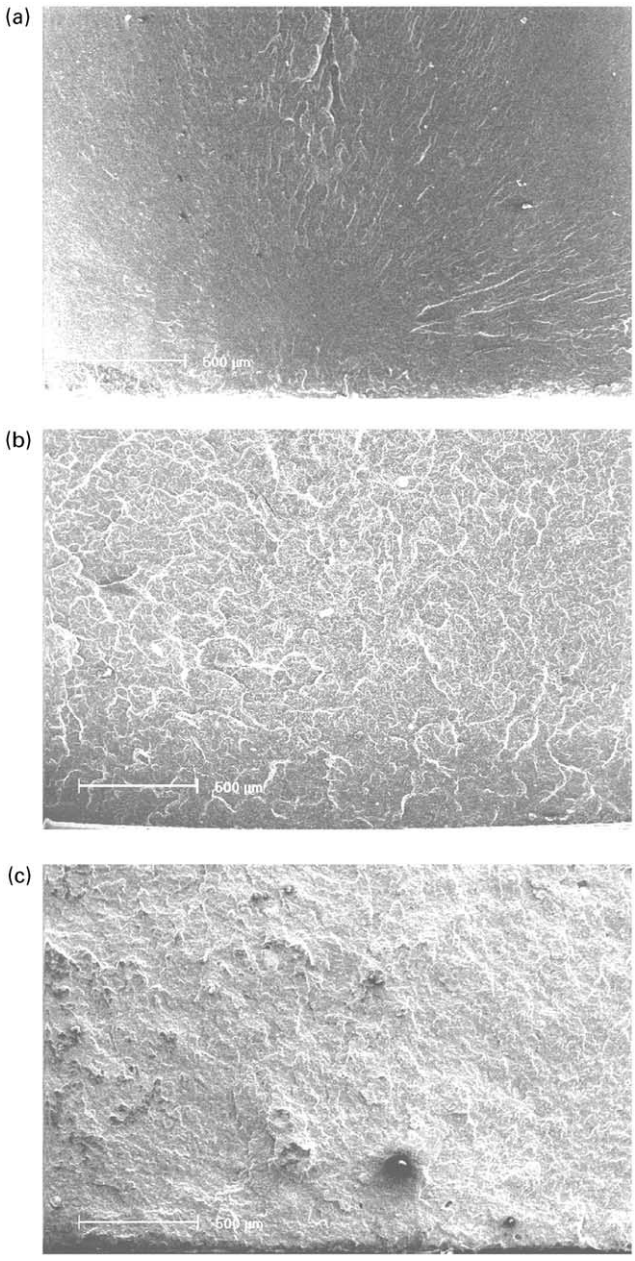


Fig. 9. SEM micrographs of Izod fracture surfaces. The notch is at the bottom of each figure and the crack propagation direction is upwards. (a) Unfilled iPP; (b) iPP + 5% CC0.7; (c) iPP + 30% CC0.7.

surfaces appeared relatively flat and no significant whitening was observed. Even in the CC0.7 blends with higher impact energy, there were few signs of extensive plastic deformation characterizing ductile fracture.

The SEM micrographs in Fig. 9 give a closer look at these Izod fracture surfaces. A common feature shared by most of the blends, including the unfilled iPP, was a fracture initiation point located around 250 μm in front of the initial notch root, roughly equal to the initial radius of curvature of the notch. This indicates that a moderate plastic zone had developed ahead of the notch and must have developed

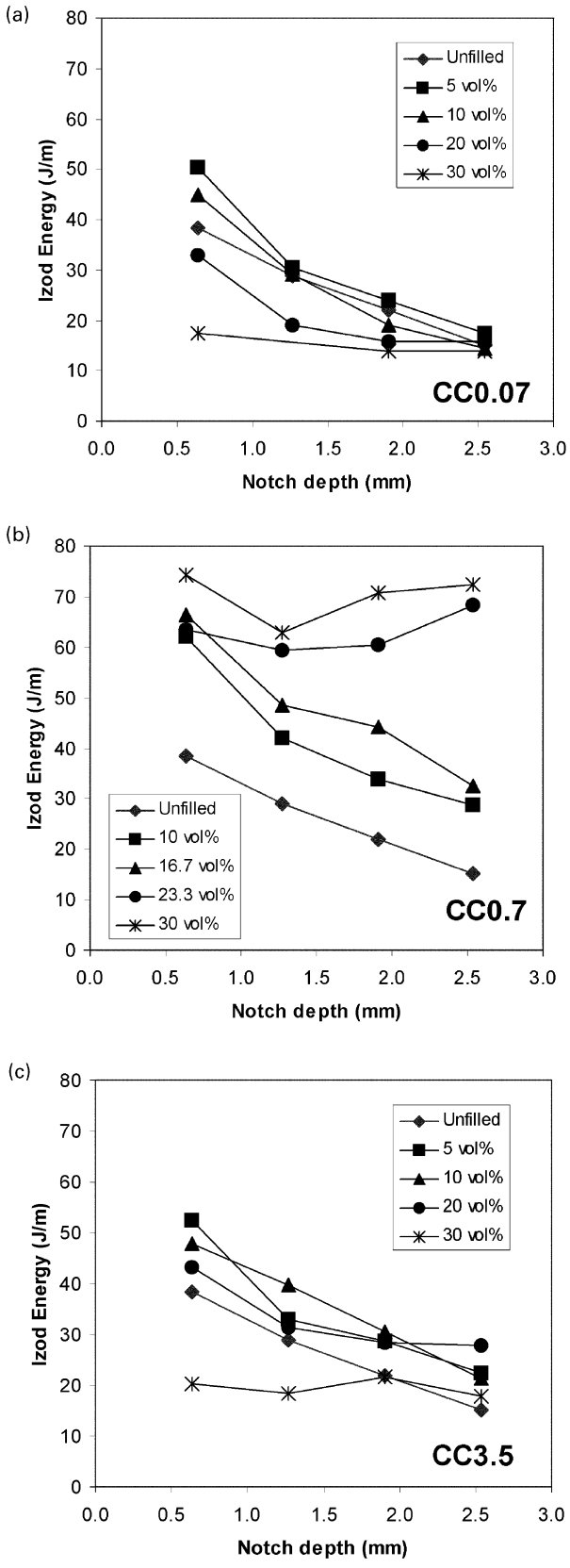


Fig. 10. Dependence of Izod impact energy on notch depth. The standard notch depth is 2.54 mm. (a) iPP + CC0.07; (b) iPP + CC0.7; (c) iPP + CC3.5.

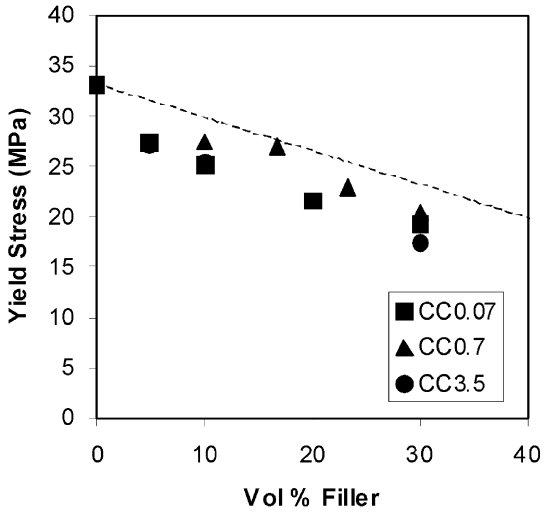


Fig. 11. Yield stress vs. volume fraction. Yield stress is taken to be the peak stress in the stress–strain curve. Shown in dashed lines is $Y = Y_0(1 - \phi)$, where $Y_0$ is the yield stress of unfilled PP and $\phi$ is the filler volume fraction.

triaxial tensile stress concentration prior to initiation of brittle behavior. This feature has been observed also in $CaCO_3$-filled Nylon [12]. The region around this fracture initiation point showed debonding of matrix from the filler. On the other hand, the remaining area of the samples (beyond 500 μm from the notch) showed neither debonding nor plastic deformation, giving a clear impression of brittle separation.

Notches concentrate stress for purely elastic response and they generate enhanced plastic strain rates at the notch root when local yielding occurs. Therefore, a number of experiments were performed to explore the effect of non-standard Izod type samples with reduced notch depths. Fig. 10 shows the dependence of impact energy on notch depth. Most of the blends, including unfilled iPP, absorb more energy as the notch depth decreases, i.e. as the stress or strain-rate concentration decreases. The blends with higher volume fraction of filler, however, maintain essentially the same impact energy independent of notch depth in the range investigated.

## 4. Discussion

### *4.1. Deformation at low strain rates*

The $CaCO_3$ filler particles played a dual role in the early deformation of the blends at low strain rates: increasing the modulus and decreasing the yield stress. The increase in modulus in the elastic region prior to particle separation showed that there was some adhesion between particles and matrix at low strains. On the other hand, the monotonically decreasing values of yield stress indicate that the adhesion is relatively weak allowing debonding to occur prior to fully developed plastic deformation. Fig. 11 is a plot of the yield stress against filler volume fraction. The experimental

values are lower than the upper bound estimate expected from the plastic stretching of the matrix ligaments formed by prior debonding of the particles, which gives a linear behavior shown by the dashed line. The observed scatter in the results is suggestive of debonding that occurs as a distributed process rather than being dependent on a single critical macroscopic condition. One way to examine the process more closely would be to measure the volumetric strain in the early stages of the stress–strain curve. Debonding leads to creation of voids, which should increase volumetric strain progressively above the elastic contribution. We are currently engaged in such an examination of volumetric strain behavior of iPP–$CaCO_3$ blends.

The critical flaw half-length, $a$, which triggers brittle response in a sample can be estimated from a Griffith-like expression [15]

$$a = \frac{JE}{\pi(1-\nu^2)(1-\phi)^2(Y_0)^2} \tag{3}$$

where $J$ is the $J$-integral toughness value; $E$, the Young's modulus; $\nu$, the Poisson's ratio; $\phi$, volume fraction of fillers; $Y_0$ is the yield stress. A global decrease in plastic resistance or yield stress could lead to enhanced toughness because a material with a fixed population of flaws is less prone to achieve a critical condition triggering brittle fracture. This is indeed shown by the samples with lower particle volume fractions that stretched much further than unfilled iPP (Fig. 3). However, the presence of larger agglomerates at high volume fraction counters the beneficial effect of reduced stress levels by acting as inclusions with sufficiently large values of $a$ to trigger brittle behavior. Using an estimated value of 0.3 for Poisson's ratio and experimental values for the other parameters in the above equation, the critical crack half-length, $a$, was calculated to be in the range 60–800 μm. Particle agglomerates observed under SEM were in this size range. Furthermore, at high filler volume fractions, it was common for several of these agglomerates to be found in close proximity in the micrographs. Thus, while smaller individual agglomerates may be tolerable in low strain rate experiments (Fig. 6(b) and (c)), larger ones or groups of small ones proved catastrophic. The relatively ductile behavior of the CC3.5 blends indicates that neither agglomeration nor irregular particle shape was a problem at the low strain rate of the tensile test.

### 4.2. J-integral toughness

The effect of filler content on the $J$-integral toughness, shown in Fig. 7, indicates an initial jump in $J$ due to the addition of a small amount of filler. The initial increase in $J$ is caused by the plastic stretch of interparticle ligaments. Adding more filler into the matrix, however, leads to a decrease in $J$. This is caused by the continual reduction in the amount of matrix polymer, the component which actually contributes to energy absorption.

Extrapolation of the trend in Fig. 7 to 0% filler content does not yield the measured $J$-integral toughness of the unfilled iPP, indicating that addition of filler produces a fundamentally different behavior. In the unfilled iPP, the material is a fully dense solid albeit with presence of internal defects due to processing. With the addition of $CaCO_3$, given that the particle–matrix adhesion is sufficiently weak to allow plastic stretch of the interparticle ligaments, the material constitution is converted into that of a cellular solid where the ligaments between the particles can plastically stretch. The same condition can be achieved by addition of rubber particles that cavitate prior to fully developed plastic deformation of the matrix. The use of rubber particles as a toughening agent is often successful because of its relative ease of dispersion when compared to the tendency of rigid fillers to cluster into agglomerates that are difficult to break during compounding. Whenever a cellular matrix with uniform dispersion is achieved, however, the appearance of significant toughening due to the stretching of these ligaments depends on the matrix properties, not on the type of filler.

### 4.3. Deformation at high strain rate

The trends of the notched Izod impact toughness values reported in Fig. 8 are not consistent with the toughness of various blends derived from the stress–strain curves in Fig. 3. For example, high volume fraction of CC0.7 increased the Izod energy considerably; the same blend fractured very early during the tensile test. The stress–strain curves of the blends with CC3.5 showed considerable strain to fracture but their Izod energies are similar to or lower than the unmodified iPP. Toughness in the tensile test (the area under the stress–strain curve) depends largely on the strain at break, which in turn is governed by the presence of flaws. Izod toughness, on the other hand, is a measure of the energy required to propagate a crack rapidly. The slow tensile test eventually probes the whole gauge volume of the specimen whereas Izod test normally only involves the plane directly ahead of the notch tip where, in a material with very low level of plastic response, the fracture becomes unstable. Moreover, the presence of the notch and especially the much higher imposed velocity result in a large value of local strain rate in the Izod experiment, orders of magnitude larger than that in the tensile test. Thus, it is not surprising that the two toughness measurements present quite different trends.

The only type of particle that enhanced impact toughness of iPP was CC0.7. Both the larger (CC3.5) and the smaller (CC0.07) particle types had a detrimental effect on the toughness. Based on these observations, the mechanism of toughening appears to be unrelated to the interparticle distance ($\lambda$) because the relationship between $\lambda$ and average particle size ($d$) is such that at the same volume fraction, blends with a smaller $d$ will have a smaller $\lambda$ [7]. If, as proposed by Wu [7], a special toughening mechanism

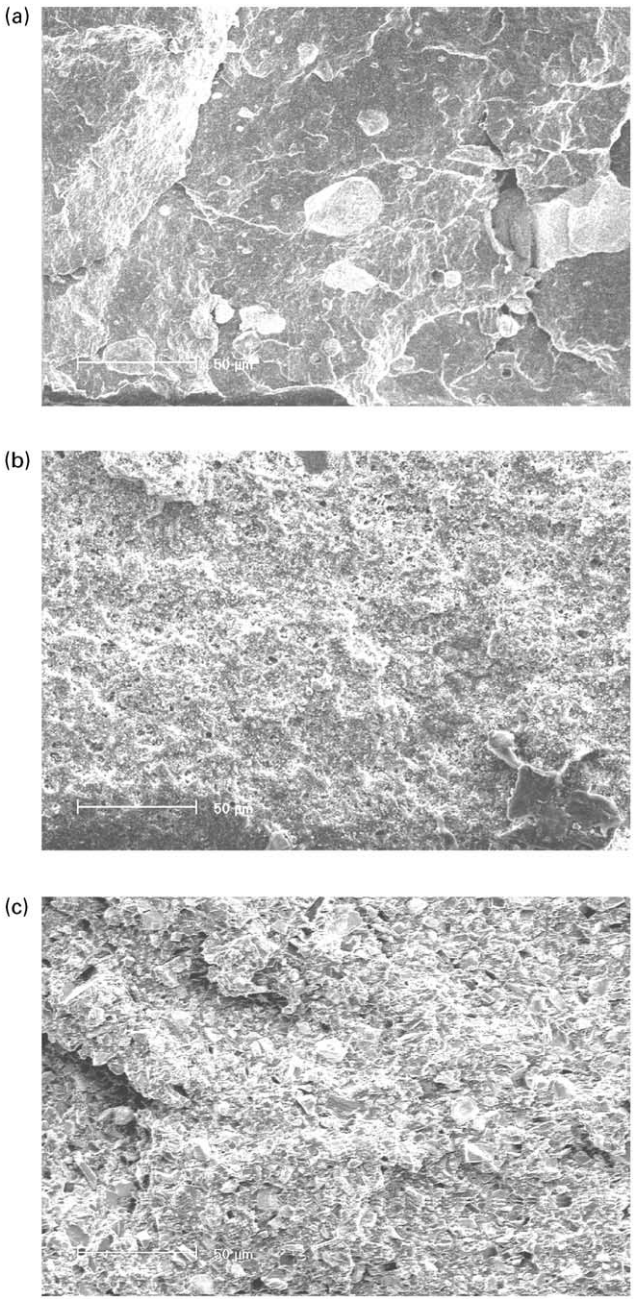


Fig. 12. SEM micrographs of Izod fracture surfaces near the notch. (a) iPP + 30% CC0.07; (b) iPP + 30% CC0.7; (c) iPP + 5% CC3.5.

becomes active below a certain critical distance $\lambda_c$, the CC0.07-filled samples should be toughened as well as the CC0.7-filled ones because $\lambda$ should be smaller at each volume fraction for the CC0.07 blends.

The impact behavior of the CC0.07-filled specimens was compromised by the ubiquitous agglomeration of the particles. An example of this is shown in Fig. 12(a) where many agglomerates larger than 25 μm were present in the CC0.07 compounds. The primary role of these agglomerates is to trigger brittle fracture. We observed consistently that the onset of crack growth in the notched Izod experiment leads to plastic notch blunting in a region just ahead of the notch radius. In this small region, the favorable mechanism of plastic deformation of the interparticle ligaments is successfully toughening the material. However, the local geometry results in an increase in stress and strain rate just under the notch root, as will be discussed in Section 4.4, rendering the specimen more susceptible to brittle fracture. The agglomerates provide a convenient trigger for brittle behavior because of their large sizes and sharp edges. In the case of the larger particle type CC3.5, shown in Fig. 12(c), the extreme irregularities in particle shapes and sizes played the same roles as agglomerates in the smaller particles. In contrast, as is also shown in Table 2, the intermediate size particle CC0.7 showed much fewer agglomerates than the other particle types did, particularly at higher filler content.

The fracture surfaces of essentially all of the notched Izod specimens tested at room temperature display a brittle mode of separation with some evidence of plastic deformation observed only very near the notch root. The fracture surface shown in Fig. 9(c) of a toughened sample, one filled with 30% filler CC0.7 particles suggests a contribution from crack deflection toughening mechanism [16]. In this process, energy is absorbed through creation of larger surface area facilitated by the specimen's internal inhomogeneity, which is associated with shunting the actual fracture plane to different levels from that of the average fracture plane.

In principle, it should be possible to produce conditions where the crack deflection mechanism is less important than the process of plastic stretch of interparticle ligament, as observed by Bartczak et al. [9–11] for $CaCO_3$ filled HDPE. We noted above that the plastic resistance of iPP is raised considerably in the local condition of high strain rate near the notch root. Raising the temperature should have the desirable effect of reducing both iPPs plastic resistance and its strain rate sensitivity. Fig. 13 shows the notched Izod impact energy for the blends containing CC0.7 particles measured at various temperatures. At 50 and 80 °C, many filled samples did not break completely and showed extensive whitening, evidence of large scale plastic deformation. The unfilled iPP, on the other hand, always produced brittle-appearing smooth fracture surfaces at higher temperatures despite the observed increase in Izod energy values. These observations are consistent with the notion that the plastic stretch of ligaments between particles in the filled compounds is now the dominant mechanism contributing to toughness.

The observed increased toughening in the CC0.7 compounds at room temperature can therefore be attributed to a combination of crack deflection and plastic deformation of interparticle ligaments. When the plastic resistance is lowered by raising temperature, the latter mechanism becomes dominant. The plastic stretch of interparticle ligaments is facilitated by debonded particles. If large particles or agglomerates are present, they act as super-critical sized

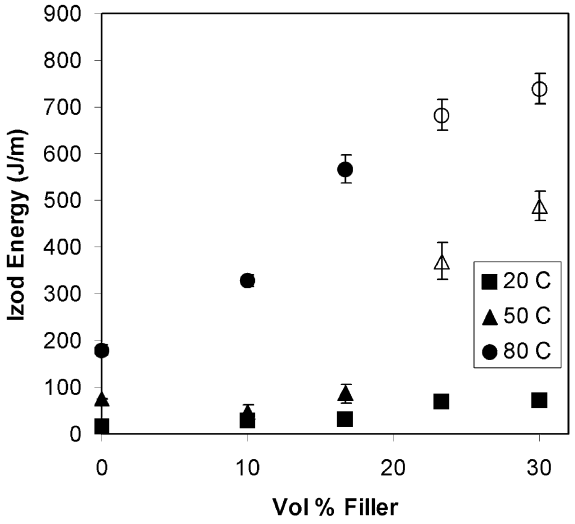


Fig. 13. Izod impact energy values for iPP + CC0.7 samples at three different temperatures. The standard notch depth was used. Open symbols indicate that the specimens did not break completely.

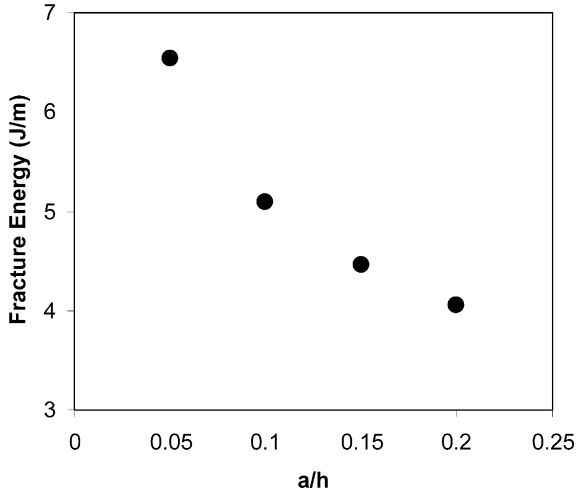


Fig. 14. Calculated fracture energy for different ratios of notch depth $a$ to specimen width $h$.

flaws and the propagating crack becomes brittle soon after initiation. Small particles are therefore potentially more beneficial as long as they do not agglomerate.

### 4.4. Analysis of the Izod experiments—effect of notch depth

The standard Izod experiment is designed to probe the fracture behavior of a material under a standard set of conditions of local stress concentration and high strain rate at the notch root. If the material behavior were purely brittle and elastic, both stress and strain would be concentrated equally. Whenever local plastic response is initiated, the concentration of stress decreases while the concentration of inelastic strain and strain rate increases. The latter effect can then elevate the plastic resistance and result in material embrittlement.

We start by considering the Izod sample first as a simple elastic cantilever beam of length $L$, thickness $b$, and width $h$ with a notch of depth $a$ having a standard notch tip radius of curvature $\rho$. If the striker is designed to strike the bar at its very end, producing a force $F$, the elastic strain energy of bending in the bar is $\beta F^2L^3/bEI$, where $E$ is the Young's modulus and $I$ is the bending moment of inertia. There will also be a component of elastic shear strain energy stored in it which, however, for the bar of standard dimension is negligible (Appendix B.1).

If the maximum force of impact is limited by a critical notch-tip tensile stress $\sigma_c$ that initiates fracture, then the strain energy of the Izod bar per unit thickness becomes at fracture, for the case of zero plastic response at the crack-tip

$$U_B = \beta\left(\frac{a}{h}\right)\left(\frac{\sigma_c}{E}\right)^2 \frac{EhL}{18}\,\frac{1}{(1+2\sqrt{a/\rho})^2} \tag{4}$$

where the factor $\beta(a/h)$ accounts for the increased compliance of the bar due to the introduction of the notch of depth $a$. The factor in the denominator of the last term is the stress concentration effect of a shallow notch of depth $a$ with a notch tip radius of curvature $\rho$ [17].

Since the energy observed in the fracture of the Izod bar involves also the fracture work $J$ at the notch plane, which is of primary interest, the total fracture energy per unit thickness, $U$, becomes

$$U = U_B + J(h - a) \tag{5}$$

where $J$ is the specific notch-plane work of fracture.

To develop some insight into these observations, we evaluate Eq. (5) for the series of Izod bars with both standard ($a = 2.54$ mm) and shorter notch depths of 0.64, 1.27, and 1.91 mm, with $L = 31.5$ mm, $h = 12.7$ mm, and $\rho = 0.25$ mm. For material properties, we take $E = 1440$ MPa (Table 3). Since the fracture surface observations indicate that the initiation sites of fracture are most often about one notch root radius beyond the actual notch surface, implying a local plastic flow induced enhancement of mean normal stress there, we take for the critical stress $\sigma_c$ the tensile yield stress $\sigma_0 = 33$ MPa (Table 3). For the specific fracture work at the notch plane for unfilled PP we take $J = 300$ J/m$^2$ (Fig. 9). Then, using these values and the enhanced compliance factors $\beta(a/h)$ [18], we determined the total Izod fracture energy values for the series of four notch depths, including the standard notch, for the unfilled iPP. The result is shown in Fig. 14. While the calculated energies are considerably lower than observed, they show a trend similar to the data for the unfilled samples in Fig. 10.

The decreasing Izod fracture energies with increasing notch depth shown in the experimental results of Fig. 10 could also be explained based on the change in local inelastic notch tip strain rates when local plastic behavior replaces elastic response. An increase in the inelastic strain rate (as notch depth increases) would evoke an increase in the plastic resistance that, in the presence of a limiting fracture stress, can result in a significant decrease in the local plastic

strain to fracture. This reduction in plastic strain would reduce the specific work of fracture $J$ [12].

The inelastic strain rate can be readily evaluated by approximating the notch as a crack. A typical strain-rate/stress relation for the plastic response of the matrix is

$$\frac{\sigma}{\sigma_0} = \left(\frac{\dot{\varepsilon}}{\dot{\varepsilon}_0}\right)^N \tag{6}$$

where $\sigma_0$ and $\dot{\varepsilon}_0$ are reference stress and strain rate values, and $N$ is a phenomenological exponent. Then, the notch tip inelastic strain rate $\dot{\varepsilon}_{nt}$ is concentrated above a nominal strain rate $\dot{\varepsilon}_0$ according to the following expression [19]:

$$\frac{\dot{\varepsilon}_{nt}}{\dot{\varepsilon}_0} = \left[A(N)\left(\frac{\sigma_B}{\sigma_0}\right)^2\left(\frac{a}{\rho}\right)\right]^{1/(1+N)} \tag{7}$$

where $A(N)$ is a function only of the exponent $N$ (Appendix B.2); $\sigma_B$, the nominal local bending stress; $\sigma_0$ is the yield stress. In the case of the Izod sample, $\dot{\varepsilon}_0$ can be taken as the local notch region elastic bending strain divided by the loading time to fracture of the sample by the striker (roughly 0.2 ms). This represents the principal rate effect of the impact experiment. The additional strain rate enhancement due to changing notch depth should then be roughly in proportion to the notch depth for typical exponent $N$ values in the range of 0.1, as is clear from Eq. (7). Thus the non-standard notches used in this study will change the notch tip strain rates only nearly linearly with notch depth, which according to Eq. (6) will produce only a very weak enhancement of the plastic resistance between the shallowest notch and the standard one. Therefore, the observed trends for $CaCO_3$-filled iPP demonstrated in Fig. 10 are principally due to an increase in stress concentration with increasing notch depth in a brittle material. The Izod test fracture behavior is mostly brittle because of the large value of $\dot{\varepsilon}_0$, which for the Izod impact experiment is orders of magnitude greater than in the standard tension experiment.

Finally, the trends shown in Fig. 10 can be analyzed in the context of the essential work of fracture (EWF) which scales directly with the remaining specimen dimension beyond the notch as has been developed by Mai and co-workers [20]. Given a plot of fracture energy versus notch depth, the EWF construction allows the calculation of essential work (the fracture energy linearly extrapolated to zero specimen length) and plastic work (derived from the slope). This construction, however, is not applicable to our system. The Mai development requires that the basic mechanism of separation be of a given type such as pure cleavage or ductile cavity growth, exhibiting the same signature along the entire length of the fracture surface. Our fractography shows a large variation from incipient ductile processes to rather smooth fracture surfaces, finally to a rough tiered type of fracture representative of crack deflection toughening, all indicating transitional forms rather than a non-changing form. Furthermore, a graphical test of the Mai approach on our results leads to negative values of essential work, evidence of the inapplicability of the procedure for the material and impact test procedure used in this work.

## 5. Conclusion

Addition of three types of $CaCO_3$ particles into iPP matrix resulted in increases in the Young's moduli. The notched Izod toughness remained essentially unchanged from the unfilled iPP value, except in the case of one particle type with average diameter of 0.7 μm, where the notched Izod toughness increased significantly at high filler content (>20 vol%). The 0.07 and 3.5 μm diameter particles' failure to toughen the matrix arises due to the presence of agglomerates and/or individual particles with dimensions larger than the critical flaw size to initiate brittle behavior. The increased Izod toughness in the compounds with 0.7 μm particles resulted from combined mechanisms of crack deflection toughening and local plastic deformation of interparticle ligaments following particle–matrix debonding. When the plastic resistance of iPP is reduced by increasing the temperature, the local plastic stretch of interparticle ligaments becomes the dominant mechanism of toughening. This points to the possibility of greater enhancement of toughness at room temperature of these filled systems using low molecular weight plasticizers or other means to reduce the plastic resistance of the matrix. From the point of view of choosing rigid particles as fillers, our results indicate that there exists an optimum window of particle size that is conducive to enhancement of toughness. Particles that are too large act as initiation sites for brittle crack behavior. On the other hand, very small particles are difficult to disperse, creating agglomerates that behave as large single particles. The optimum size depends on the processing of the compounds and on the tolerance of the polymer matrix to large inclusions.

The $J$-integral toughness increased with initial addition of $CaCO_3$ but decreased with subsequent addition. This observation is consistent with the notion that the addition of filler particles changes the material constitution from that of a fully dense solid to one with quasi-regularly distributed voids. The formation of such a cellular solid was observed in relatively slow strain rate experiments but almost not at all in the room-temperature Izod impact experiments. More detailed studies of the various steps in the toughening mechanism—for example, the dependence of the debonding and the interparticle ligament stretching processes on rate and local state of stress—are needed before these concepts can be applied in a reliable way to improve the impact toughness of thermoplastic polymers.

## Acknowledgements

This research was supported by the NSF MRSEC program through the Center of Materials Science and Engineering at MIT from Grant DMR-98-08941. We

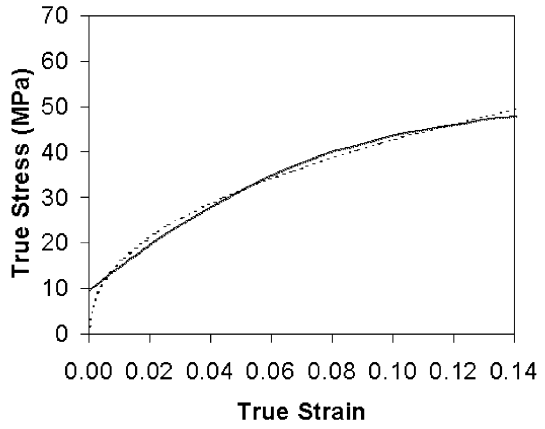


Fig. 15. The plastic portion of the stress–strain curve of unfilled iPP in uniaxial compression. The dotted line is the fitted behavior for hardening matrix.

acknowledge helpful discussion with D.M. Parks and F.A. McClintock.

## Appendix A. Compression test of unmodified iPP

Compression experiments were performed to obtain power law parameters used in the *J*-integral calculation. Molded unmodified iPP flexural bars were machined into cylindrical specimens of 7 mm radius and 3.2 mm thickness. The samples were preconditioned previous to testing to minimize the yield phenomenon; this was done by annealing the samples at 150 °C for 2 h, quenching them in liquid nitrogen, and testing them immediately after they reach room temperature. Samples were compressed at constant true strain rate of $0.01\ s^{-1}$ using Instron 1350 with servohydraulic controls. An extensometer with a gauge length of 12.7 mm was used.

The plastic portion of the resulting true stress–true strain curve is fitted to the power law strain hardening expression: $\varepsilon = \alpha\varepsilon_0(\alpha/Y_0)^n$. Fig. 15 shows the plastic part of stress–strain curve and the fit. $Y_0$ in this case is taken as the departure from linear (elastic) behavior; the average value of $Y_0$ was 16.0 MPa. The other parameters, $n$ and $\alpha\varepsilon_0$, are determined through fitting: $n = 2.16$ and $\alpha\varepsilon_0 = 0.0105$.

## Appendix B

### *B.1. Elastic–brittle response*

Elementary beam theory for the bending of a cantilever beam of length $L$, width $h$, and thickness $b$, subjected to an end load $F$ in the stiff plane of the bar will give a load-point bending displacement

$$\delta_B = \frac{FL^3}{3EI} \tag{A1}$$

where $E$ is the Young's modulus and $I$, the moment of inertia. If a notch of depth $a$ is present on the side of the applied load, the bar will acquire additional flexibility that can be characterized by a factor $\beta(a/h)$ [18], giving

$$\delta_B = \beta\left(\frac{a}{h}\right)\frac{FL^3}{3EI} \tag{A2}$$

The elastic strain energy of bending then becomes:

$$U = \beta\left(\frac{a}{h}\right)\frac{F^2L^3}{Eh^3b} \tag{A3}$$

The peak load is limited by a fracture process at the notch root when the local stress reaches $\sigma_c$ given by the local bending stress concentration as [17]

$$\sigma_c = \frac{6FL}{h^2b}(1 + 2\sqrt{a/\rho}) \tag{A4}$$

where $\rho$ is the notch radius of curvature. Substitution of this expression into Eq. (A3) gives the bending elastic strain energy per unit thickness as

$$U_B = \beta\left(\frac{a}{h}\right)\left(\frac{\sigma_c}{E}\right)^2\frac{EhL}{18}\frac{1}{(1 + 2\sqrt{a/\rho})^2} \tag{A5}$$

The evaluation of this expression requires the evaluation of the factor $\beta$ [18]. The values are 1.025, 1.070, 1.143, and 1.233 for $a/h = 0.05$, 0.1, 0.15, and 0.2, respectively.

Finally, the bent Izod cantilever is very stubby and is sheared in addition to being bent, requiring the elastic strain energy of shear to be assessed as well. From beam theory, this shear strain energy $U'$ is

$$U' = \frac{F^2L}{2hb\mu} \tag{A6}$$

where $\mu$ is the shear modulus, which for an isotropic solid with a Poisson's ratio $\nu$ is $E/2(1 + \nu)$. The ratio of $U'$ to $U$ then becomes

$$\frac{U'}{U} = \frac{1 + \nu}{2}\left(\frac{h}{L}\right)^2 \tag{A7}$$

For an Izod bar, this will give a value of around 0.1. Furthermore, while the bending strain energy is accentuated by the notch, the shear strain energy will not.

### *B.2. Strain rate enhancement at notch tip*

When a limited amount of local plasticity is present at the notch tip as our results suggest, then the local enhancement of the inelastic strain rate becomes of interest. While the actual elastic-plastic-rate dependent material response is complex and requires numerical solution, a useful limiting assessment of the effect was provided by Rice [19] which is based on approximating the notch with a crack and gives

$$\dot{\varepsilon}_{nt} = \dot{\varepsilon}_0\left[\frac{(N + 0.5)(N + 1.5)\Gamma(N + 0.5)}{\Gamma(0.5)\Gamma(N + 1)}\frac{K_I^2}{\sigma_0^2\rho}\right]^{1/(1+N)} \tag{A8}$$

for a power law constitutive relation given by Eq. (6) in the text, where $\Gamma(x)$ is the gamma function and $K_I = \alpha\sqrt{\pi a}$ is the mode $I$ stress intensity factor. Since the multiplicative factor involving the gamma functions and exponent $N$ is a material parameter, we have replaced it with $A(N)$ in Eq. (7) in the text.

## References


[1] Liang JZ, Li RKY. J Appl Polym Sci 2000;77:409.
[2] Rothon R. Particulate-filled polymer composites. New York, NY: Wiley, 1995.
[3] Mitsuishi K, Kodama S, Kawasaki H. Polym Engng Sci 1985; 25:1069.
[4] Levita G, Marchetti A, Lazzeri A. Polym Compos 1989;10:39.
[5] Jancar J, DiBenedetto AT. Polym Engng Sci 1993;33:559.
[6] Demjen Z, Pukanszky B, Jozsef N. Composites Part A 1998;29:323.
[7] Wu S. J Appl Polym Sci 1998;35:549.
[8] Muratoglu OK, Argon AS, Cohen RE, Weinberg M. Polymer 1995;36:921.
[9] Bartczak Z, Argon AS, Cohen RE, Weinberg M. Polymer 1999; 40:2331.
[10] Bartczak Z, Argon AS, Cohen RE, Weinberg M. Polymer 1999; 40:2347.
[11] Bartczak Z, Argon AS, Cohen RE, Weinberg M. Polymer 1999; 40:2367.
[12] Wilbrink MWL, Argon AS, Cohen RE, Weinberg M. Polymer 2001;42:10155.
[13] Wu X, Zhu X, Qi Z. In: Young RJ, editor. Eighth International Conference on Deformation, Yield, and Fracture of Polymers, vol. 78. 1991. p. 1.
[14] Kumar V, German MD, Shih CF. An engineering approach for elastic plastic fracture analysis (NP-1931 research project 1237-1). Palo Alto, CA: Electric Power Research Institute, 1981.
[15] Anderson TL. Fracture mechanics. 2nd ed. Boca Raton, FL: CRC Press, 1995.
[16] Argon AS. Fracture: strength and toughness mechanisms. In: Chou TW, editor. Comprehensive composite materials, vol. 1. Oxford, UK: Pergamon Press, 2000. p. 798.
[17] Neuber H. Theory of notch stresses: principles for exact stress calculation. Ann Arbor, MI: Edwards, 1946.
[18] Tada H, Paris PC, Irwin GR. The stress analysis of cracks handbook. 2nd ed. St Louis, MO: Paris Productions Inc, 1985.
[19] Rice JR. In: Liebowitz H, editor. Fracture: an advanced treatise, vol. II. New York, NY: Academic Press, 1968. p. 292.
[20] Fasce L, Bernal C, Frontini P, Mai YW. Polym Engng Sci 2001;41:1.